The Meteoritical Society

Meteoritics & Planetary Science 44, Nr 7, 1019–1032 (2009)
Abstract available online at http://meteoritics.org

Trace element chemistry of Cumulus Ridge 04071 pallasite with implications for main group pallasites

Lisa R. DANIELSON[1*], Kevin RIGHTER[2], and Munir HUMAYUN[3]

[1]Mailcode JE23, NASA Johnson Space Center, 2101 NASA Parkway, Houston, Texas 77058, USA
[2]Mailcode KT, NASA Johnson Space Center, 2101 NASA Parkway, Houston, Texas 77058, USA
[3]National High Magnetic Field Laboratory and Department of Geological Sciences, Florida State University, Tallahassee, Florida 32310, USA
[*]Corresponding author. E-mail: lisa.r.danielson@nasa.gov

(Received 06 November 2008; revision accepted 11 May 2009)

Abstract–Pallasites have long been thought to represent samples from the metallic core–silicate mantle boundary of a small asteroid-sized body, with as many as ten different parent bodies recognized recently. This report focuses on the description, classification, and petrogenetic history of pallasite Cumulus Ridge (CMS) 04071 using electron microscopy and laser ablation ICP-MS. Most olivines are angular in CMS 04071, but there are some minor occurrences of small rounded olivines, such as in the Eagle Station pallasite. Olivine, chromite, and metal compositions indicate that CMS 04071 can be classified as a Main Group pallasite. The kamacite/taenite partition coefficients (D) for highly siderophile elements (HSE) are all close to 1, but comparison with previous studies on iron meteorites and pallasites shows that variation of some D values is controlled by the Ni content of taenite. $D(HSE)_{metal/sulfide}$ for Re, Cu, and Cr all are <1, indicating chalcophile behavior for these three elements, in agreement with experimental $D_{metal/sulfide}$. $D(HSE)_{metal/olivine}$ are variable, which is perhaps due to small metallic inclusions in the olivine that are present to variable extents in different pallasites. All of these data, together with results from previous studies, indicate that the CMS pallasites were likely formed at the core-mantle boundary of a small asteroid, but not necessarily related to the core that produced the IIIAB irons. In addition, they share a similar volatile element depletion to HEDs that is distinct from other bodies such as Earth, Mars, Angrite Parent Body, and the parent body of the brachinites.

INTRODUCTION

Pallasites are stony iron meteorites that are widely thought to represent a mixture of mantle (olivine) and core (FeNi metal) materials (e.g., Mittlefehldt et al. 1998). A link between pallasites, IIIAB irons, and HED meteorites was proposed on oxygen isotopic measurements on these classes of meteorites (Clayton and Mayeda 1996), and the chemical similarity between IIIAB and pallasite metal (Scott 1977). However, recent high-resolution oxygen isotope analyses have shown that pallasites and HEDs have subtly different oxygen isotopic values (Greenwood et al. 2006). Also, pallasite metal has a different Re-Os age (Shen et al. 2002) and cooling rate (Yang and Goldstein 2006) than IIIAB irons. Despite this, detailed studies of pallasites have revealed as many as seven different parent bodies, making any new pallasite finds of great interest to the meteorite community. For example, Main Group pallasites were defined by Scott (1977a), along with the Eagle Station Trio and pallasites with anomalous olivine composition (Buseck 1977; Scott 1977a). Since then, pallasites with anomalous metal contents have been discovered (Wasson and Choi 2003) as well as a pallasite (for example, Milton) with anomalous oxygen isotopic composition (Jones et al. 2003). In addition to these five groups, there are 2 pyroxene pallasites that are not related to each other (Vermilion and Yamato 8251; Boesenberg et al. 2000; Yanai and Kojima 1995). Further, Ziegler et al. (2007) report distinct oxygen isotopic values for two subgroups within the Main Group pallasites. Altogether, these new results suggest pallasites are derived from several different parent bodies, perhaps as few as 5–7 (Boesenberg 2000 and personal communication), though ^{53}Mn-^{53}Cr chronological relations may require as many as ten distinct parent bodies (Tomiyama and Huss 2006; Tomiyama et al. 2007). These recent developments make unraveling pallasite petrology and origin all the more intriguing and of interest to defining the nature of the pallasite formation process.

This report focuses on the description, classification, and

© The Meteoritical Society, 2009. Printed in USA.

Fig. 1. Photograph of hand sample of CMS 04071, 0 with 1 cm cube for scale (AMN 2005).

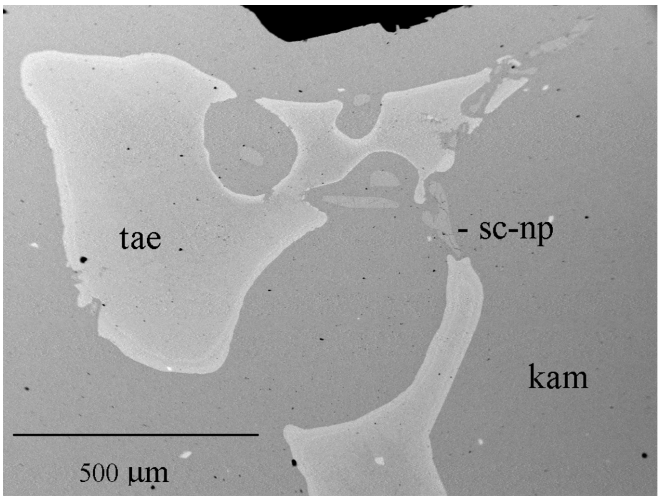

Fig. 2. BSE image of metallic region in CMS 04071. Abbreviations are tae: taenite, kam: kamacite, sc-np: schreibersite and nickelophosphide.

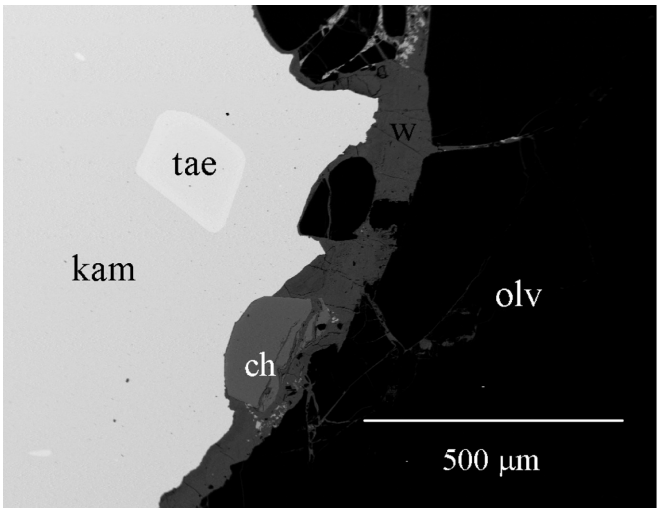

Fig. 3. BSE image of metal-silicate interface. Abbreviations are kam: kamacite, tae: taenite, ch: chromite, olv: olivine, w: weathering product.

petrogenetic history of pallasite Cumulus Ridge (CMS) 04071, found on the ANSMET 2004–2005 expedition. It is paired with CMS 04061–04079, one of 18 pairs, consisting of a total of 170.55 kg in recovered mass (Table A1), with all pieces exhibiting B/C weathering and A fracturing classes (AMN 2005). Although there have been other pallasites discovered in Antarctica (Thiel Mountains, Queen Alexandra Range [QUE] 93544, Pecora Escarpment [PCA] 91004, Yamato 8451 and 74044), the CMS pairing group comprises the largest pallasite recovered from Antarctica. We will report here the mineralogy and texture of CMS 04071, as well as detailed analyses of trace elements in individual phases. All data will be used to place CMS 04071 in the context of the various pallasite groups and to infer its possible origin and history. Initial results of our investigations of this pallasite were reported earlier (Danielson et al. 2006).

SAMPLE DESCRIPTION

The sample investigated is a thick slice (CMS 04071, 9), approximately 1 cm^2 in polished area (Fig. 1). Six separate phases comprise the metal and oxide fraction of the pallasite (Table A2), kamacite, taenite, troilite, schreibersite, nickelphosphide, and chromite. Kamacite is the most abundant metallic phase, occurring in millimeter-scale interconnected networks. The kamacite interior exsolved both taenite and schreibersite-nickelphosphide (Figs. 2 and 3). Regions of sulfide and phosphide are also abundant in areas several millimeters in size. Texturally, it appears that iron-rich metal formed an immiscible liquid with sulfide and phosphide. Olivines are most commonly rounded in this section and rimmed by a Fe-rich phase (Fig. 3), which also commonly contains chromites. This rim could represent weathering products, consistent with hand sample observations of CMS pallasites reported in AMN (2005).

ANALYTICAL METHODOLOGY

Major elements were determined by electron microprobe

analyses, using the Cameca SX100 at NASA JSC, with a 15 kV accelerating voltage and 20 nA sample current. Standards include both natural (kaersutite, wollastonite, chromite, rutile, olivine, rhodonite, potassium feldspar, albite) and synthetic (Co metal, NiO) standard materials. Counting times for major elements were typically 10 s, and as long as 120 s for low concentrations of Cr or Mn in silicates and oxides. PAP ϕ–ρ–Z corrections were used in the data reduction (Pouchou and Pichoir 1991).

Trace element microanalysis was performed using a New Wave UP213 (213 nm UV) laser ablation system coupled to a Finnigan Element™ at the NHMFL, FSU, following procedures modified from Campbell and Humayun (1999) and Humayun et al. (2007). Elemental abundances were determined in line scan mode, from the isotopes: ^{53}Cr, ^{57}Fe, ^{59}Co, ^{60}Ni, ^{63}Cu, ^{69}Ga, ^{74}Ge, ^{75}As, ^{95}Mo, ^{102}Ru, ^{103}Rh, ^{105}Pd, ^{184}W, ^{185}Re, ^{192}Os, ^{193}Ir, ^{195}Pt, and ^{197}Au. Ablated tracks across individual mineral grains ranged from 100 µm to 2.36 mm long, and 30 to 110 µm wide, depending on the grain size. Silicates and oxides were analyzed with ~80–110 µm diameter tracks scanned at 10 µm/s, and metals, phosphides and sulfides were analyzed with ~30 µm diameter tracks scanned at 5 µm/s, using 10 Hz laser repetition rate and 50% power output. The NIST SRM 1263a steel (for Cr, Fe, Co, Mo, W), pyrite (S), and the iron meteorites North Chile (Filomena) and Hoba (for Co, Ni, Ga, Ge, Re, Os, Ir, Pt and Au) were used as standards (Campbell and Humayun 1999; Campbell et al. 2002; Humayun et al. 2007). Elemental abundances (Co, Ni, Ga, Ge, Re, Or, Ir, Pt, Au) of North Chile (Filomena) are derived from extensive neutron activation analyses (NAA) of this meteorite (Wasson et al. 1989) and, therefore, allow accurate inter-comparison between our laser ablation ICP-MS (LA-ICP-MS) data and NAA data available in the literature. An example of the application of LA-ICP-MS analysis of siderophile elements in bulk IVB iron meteorites with comparison to previous NAA data is provided by Campbell and Humayun (2005). However, the application of LA-ICP-MS to the analysis of ataxites is more straightforward than its application to the analysis of kamacite-taenite bearing metals, where accurate modes are also required. An example of an analytical track is given in Fig. A1, and includes kamacite and taenite. Observed compositional zoning at the phase boundaries is smaller scale than the analytical spot size, so caution should be taken in interpreting results from zoned regions. In order to measure phases not affected by secondary post-crystallization processes, trace element abundances were extracted by using average values of elements for flat portions of each traverse and by using spot analyses in phase interiors. Back-scattered electron and scanning electron microscopy images show the locations of various tracks completed in this study (Figs. 4a and 4b). Results for individual phases are reported in Tables 1–4, Table A3.

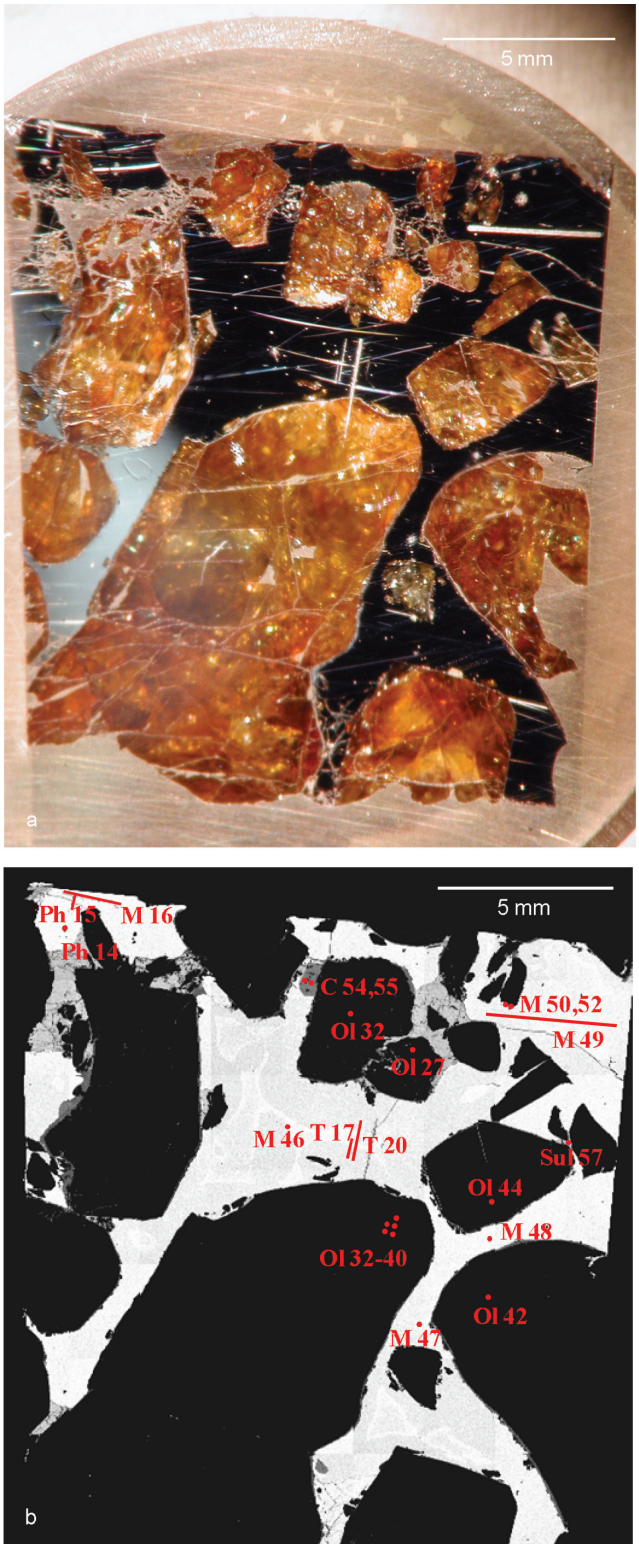

Fig. 4. a) Photograph of analyzed section of CMS 04071, 9; right edge of sample is approximately 1.5 cm in length. b) Cr Ka X-ray map of CMS 04071 ,9 showing locations of laser tracks and point analyses from the LA-ICP-MS analysis; note 5 mm scale bar at top of image.

Table 1. Averaged kamacite and taenite analyses used to calculate the bulk metal composition for CMS 04071. Fe and Ni contents in wt%, all others in ppm.

	Kamacite	Taenite	Bulk metal
Cr#	0.93	91.6	28.1
Fe	92.89	80.05	89.04
Co	5560	2880	4756
Ni	6.55	19.7	10.50
Cu#	70.6	139.7	91.33
Ga#	18.4	9.2	15.64
Ge#	38.2	16.7	31.8
Mo	4.16	5.52	4.57
Ru	1.66	4.20	2.42
Rh	0.80	1.25	0.94
Pd	3.49	10.37	5.55
W	0.14	0.14	0.14
Re	0.07	0.06	0.067
Os#	0.035	0.017	0.030
Ir#	0.0097	0.0048	0.008
Pt	1.62	1.92	1.71
Au	2.77	5.48	3.58

#Analyses from T17, and all others from T20.

RESULTS

Classification of pallasites is usually made using metal and olivine compositions (e.g., Scott 1977a; Choi and Wasson 2003). Pallasites contain both kamacite and taenite, so the bulk metal composition will be a combination of these two phases. Since we have analyses of both and a measurement of modal amounts of taenite (30 ± 5%) and kamacite (70 ± 5%) present in our section (using the BSE map and digital imaging), we calculated the bulk metal composition (Table 1). The accuracy of this bulk composition depends strongly on the mode used; our estimate nearly overlaps previous measurements of kamacite in pallasites comprising 52 to 63% of the metal phases (Massalski and Park 1964). Comparison of this bulk metal composition to that for other pallasites shows that it is similar to the metal composition of many Main Group pallasites (Fig. 5). However, the bulk metal inferred for CMS 04071 (Table 1) plots systematically lower in Co, Ga, and Ge, and higher in Au (and Ni) within the distribution of the Main Group pallasites (Fig. 5). Although this could be caused by an overestimation of the taenite modal abundance in our section, a kamacite content as high as 80–90% is outside the range measured in any pallasite previously. Comparison of olivine and chromite major element compositions for Main Group, Eagle Station Trio and anomalous olivine pallasites shows that CMS is similar to Main Group pallasites in this respect as well (Fig. 6).

Textural studies of pallasites (Scott 1977b) indicate three different pallasite types including those with angular olivines (e.g., Eagle Station, Dora), rounded olivines (e.g., Brenham, Springwater, Thiel Mountains), and those with both types (e.g., Phillips County, Molong). Although rounded olivine is the most common in this section, some angular olivine is also present and may be more abundant in the meteorite than is represented in this section (as in Fig. 1). Therefore, the CMS pallasites contain both textural types of olivines and are texturally most similar to pallasites with equi-axed large olivines and angular submillimeter olivines (Figs. 1 and 4a) such as Salta (Imilac) or Molong (Scott 1977b).

Closure temperatures were calculated for CMS 04071 using the approach of Seifert et al. (1988) (Equations 1 and 2 below), in which the exchange equilibria between olivine and metal are used as a thermometer:

$$Ni_2SiO_4 + 2Fe = Fe_2SiO_4 + 2Ni$$

$$Co_2SiO_4 + 2Fe = Fe_2SiO_4 + 2Co$$

$$\ln K_D^{ol-met} = \frac{1}{2}\Delta G^o_{0,T}/RT - In\left(\frac{\gamma_M^{met}\cdot\gamma_{Fe}^{ol}}{\gamma_M^{met}\cdot\gamma_M^{ol}}\right) \quad (1)$$

$$K_D = \frac{X_M^{met}\cdot X_{Fe}^{ol}}{X_{Fe}^{met}\cdot X_M^{ol}} \quad (2)$$

The activity coefficients (γ) and $\Delta G^o_{0,T}$ are taken from Seifert et al. (1988). Using our metal and olivine analyses (mole fraction, X) to calculate distribution coefficients, K_D, we calculate closure temperatures between 800 and 1000 °C. These closure temperatures are comparable to the range measured for other pallasites: 700–1000 °C (Seifert et al. 1988). The values are also consistent with the idea that metal-olivine equilibria closed at slightly higher temperatures than the later kamacite-taenite exsolution in metallic phases.

Cooling rates for pallasites have fallen into two groups, based on trace element zoning patterns in olivine (Tomiyama and Huss 2006; Tomiyama et al. 2007) and metal exsolution (Fe-Ni, 400–750 °C) (Yang and Goldstein 2006). Slow cooling rates (2–10 °C/Myr) were derived by Yang et al. (2008), and are different from those determined using the same approach for IIIAB irons (~100 °C/Myr) (Yang and Goldstein 2006), leading Yang and Goldstein (2006) to conclude Main Group pallasites did not form at the IIIAB core-mantle boundary. On the other hand, very rapid cooling rates have been determined looking at Cr and Mn zoning in olivines (~10^6 °C/Myr, applicable to temperature ranges 600–1100 °C) (Tomiyama and Huss 2006; Tomiyama et al. 2007). Unfortunately, the CMS pallasite exhibits zoning (e.g., Cr, Co, Ni, Cu, W, Re) across multiple phases in metals, which may be the result of diffusion on quench or post quench magmatic interaction. Thus the cooling rate history of this meteorite will be difficult to determine and may not provide new insights into the cooling rate discrepancy between IIIAB irons and pallasites as identified by Yang and Goldstein (2006).

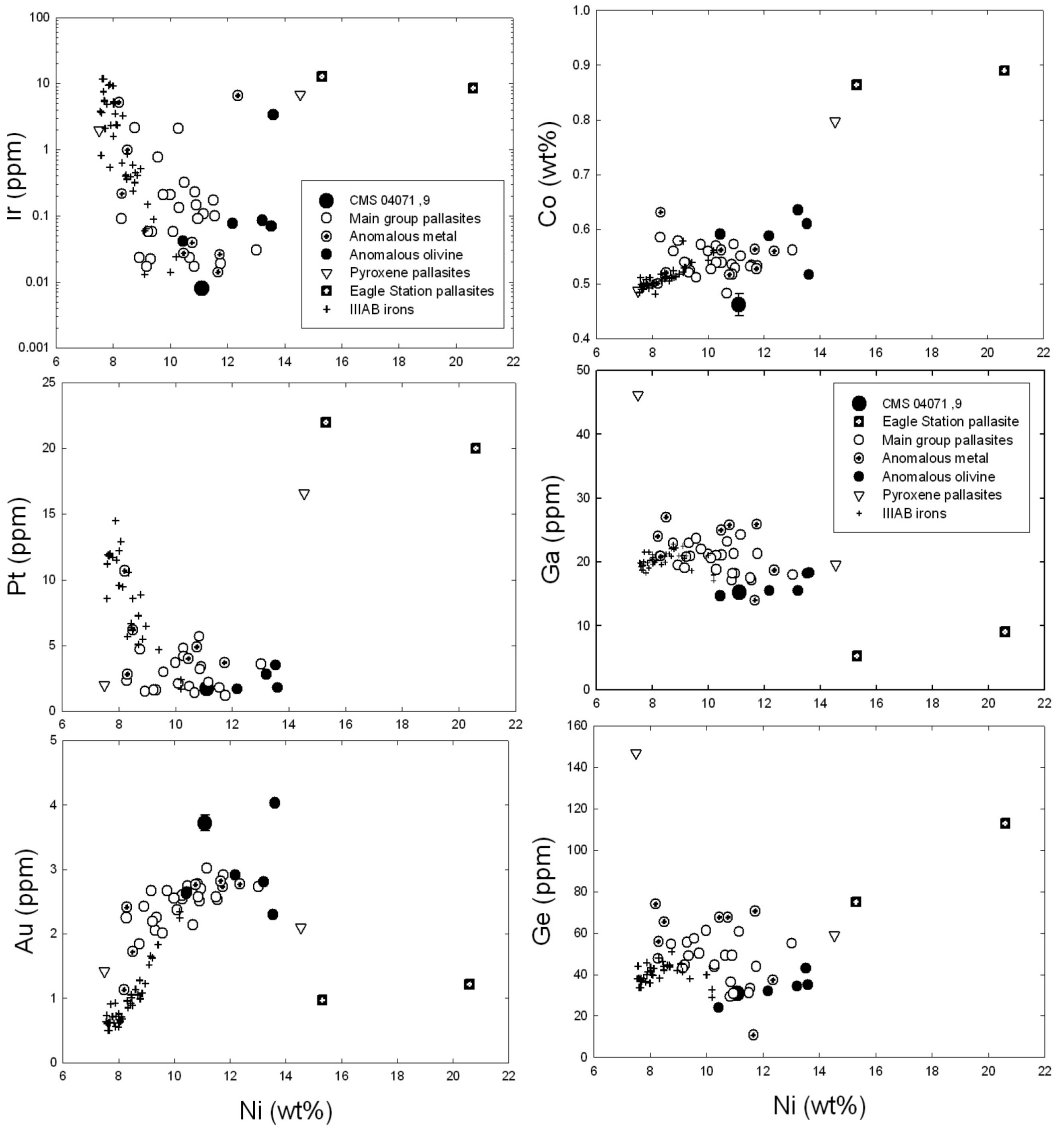

Fig. 5. Metal trace element contents for CMS 04071 compared to data from Wasson and Choi (2003) and Lauretta et al. (2006) for Fukang and other pallasite groups (main group, anomalous metal, anomalous olivine, pyroxene pallasites, and Eagle Station Trio pallasites), and to IIIAB irons (Malvin et al. 1984; Wasson et al. 1989, 1998). Ni plotted on the x-axis as an indicator of fractional crystallization processes. Co, Ga, and Ge exhibit weak compatibility during magmatic fractionation, Ir and Pt are strongly compatible, and Au is incompatible. CMS is part of a coherent magmatic trend including the IIAB irons and main group pallasites. Anomalous metal pallasites are Argonia, Brenham, Glorieta Mountain, Huckitta, Krasnojarsk, and Pavlodar; anomalous silicate pallasites are Phillips County, Rawlinna, Springwater, and Zaisho; Eagle Station pallasites are Cold Bay and Eagle Station; after Wasson and Choi, 2003. Error on CMS 04071 analyses reflects the uncertainty in modal percentage of kamacite, which is estimated to be 70 ± 5%.

Table 2. Siderophile element compositions in olivine, in ppm by weight. Italicized values are detection limits reported in place of element concentration.

	Ol 27	Ol 32	Ol 34	Ol 36	Ol 38	Ol 40	Ol 42	Ol 44
Si	221100	216000	212700	212000	215400	214500	218300	213900
Cr	81	110	122	122	125	128	99	160
Co	5.78	4.99	5.92	6.04	6.17	6.27	5.49	22.0
Ni	15.0	12.8	13.0	11.7	11.4	11.3	12.3	75.9
Cu	0.018	*0.057*	*0.052*	*0.054*	*0.056*	*0.055*	*0.062*	0.178
Ga	0.017	0.087	0.087	0.076	0.075	0.072	0.041	0.116
Re	*0.00003*	*0.00009*	*0.00005*	*0.00004*	*0.00009*	*0.00004*	*0.00004*	0.00014
Pt	*0.0003*	*0.0004*	*0.0003*	*0.0003*	*0.0003*	*0.0003*	*0.0004*	0.00041
Au	*0.0008*	*0.0009*	*0.0008*	*0.00009*	*0.0009*	*0.0009*	*0.0010*	0.00098

Table 3. Trace element analyses for chromite, in ppm. Italicized values are detection limits.

	C 54	C 55
Cr	502000	518000
Fe	227000	227000
Co	160	110
Ni	1070	1660
Cu	0.527	0.497
Ga	56.6	57.4
Mo	*0.1*	*0.1*
W	*2*	*1*
Re	*0.015*	*0.020*
Os	*0.0005*	*0.0003*
Ir	*0.0004*	*0.0003*
Pt	0.0028	0.0078
Au	0.017	0.007

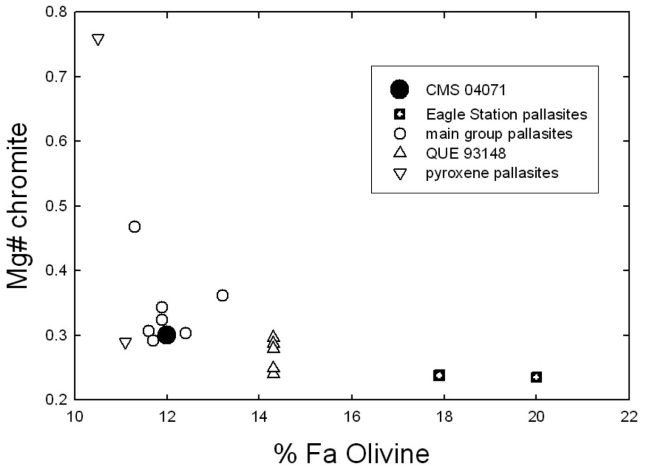

Fig. 6. Olivine and chromite compositions for main group pallasites, Eagle Station Trio, QUE 93148, and pyroxene pallasites in comparison to the CMS 04071 pallasite (data from Wasson and Choi 2003; Goodrich and Righter 2000; Wasson et al. 1999; Mason 1963; Bunch et al. 1971, and this study). Eagle Station pallasites are Cold Bay and Eagle Station; after Wasson and Choi 2003.

DISCUSSION

Trace Element Systematics

Distribution Between Metal Phases—Taenite and Kamacite

Distribution of elements between taenite and kamacite has been the focus of previous work (Hirata and Nesbitt 1997; Campbell and Humayun 1999; McDonough et al. 1999; Hsu et al. 2000; Mullane et al. 2004; Ash et al. 2007; Watson et al. 2007, 2008;), but some disagreement exists, as does a general understanding of the variation in distribution coefficients by element. Kamacite, taenite, and phosphide have similar relative trace element abundances (Fig. 7 and Tables 1, A3). Metallic phases in CMS 04071 are strongly depleted (relative to CI chondrites and Fe) in Os, Re, and Ir, slightly depleted in Pt, and slightly enriched in Ru, Rh, Au, and Pd. Low Ir with high Au is opposite from observed abundances in Esquel (Ulff-Møller et al. 1998), and a measure of bulk sulfur content of CMS 04071 metal would be necessary to address the hypothesis of S-rich metallic liquids that left the pallasite region. These depletion/enrichment patterns most likely are controlled by solid metal–liquid metal partitioning during magmatic fractionation of the metallic core (see below), where pallasite metal may represent residual liquids from a IIIAB-like core (Wasson 1999).

In addition, $D(Os, Re, Pt, Ir, Au)_{taenite/kamacite}$ are <1. This is lower than in previous studies for IAB and IIE irons, in which D values are between 1 and 2 (Hirata and Nesbitt 1997; Hsu et al. 2000), but similar to values measured for IIIAB irons (McDonough et al. 1999). Similarly, $D(Ru, Rh, Pd)_{taenite/kamacite}$ are all >1 for CMS 04071, as are values measured by McDonough et al. (1999), Campbell and Humayun (1999) and Hirata and Nesbitt (1997). In addition to the HSE, taenite/kamacite measurements in this study yield similar results to these previous studies for Cu, Ni, W, Ga, Ge, and Co (Fig. 7).

Previous studies have shown that some variation in partition coefficients between taenite and kamacite could be due to differences in ionic radii and atomic radii, or possibly temperature (Mullane et al. 2004; Watson et al. 2008), but another important factor with respect to some elements is the concentration of Ni in the taenite (which can vary between 6 and 40%, depending upon the temperature). For example, Cu and Au both show a positive dependence upon the amount of Ni in taenite (Fig. 8). Pt dependence is uncertain and may require additional research to clarify, because the measurement of Hirata et al. (1997) is outside of a possible trend defined by several other studies (Fig. 8). Pd, Ru, Rh, Os, and Ir do not show much variation or dependence on Ni, and our new measurements are consistent with previous work.

Distribution Between Metal and Sulfide

$D(HSE)_{metal/sulfide}$ ranged from ~10 to 100 (Fig. 9a). Also, $D(HSE)_{metal/sulfide}$ and $D(HSE)_{metal/chromite}$ are > 1 for Os, Ir, Pt, and Au. Two elements, Cu and Cr, exhibit chalcophile behavior (D metal/sulfide <1) in agreement with the results of Chabot et al. (2004). In fact, metal-sulfide liquid partitioning experiments by Chabot et al. (2004) for high S liquids (mole fraction of sulfur in the metal ~0.5) agree with the results for $D_{metal/sulfide}$ for most elements (Fig. 9a). The exceptions are Os, Re, and Ir for which $D_{metal/sulfide}$ are several orders of magnitude less than both the experimental values and than in IAB irons, where $D(Re,Os)_{metal/troilite} = 10^3–10^4$ (Shen et al. 1996). This is due to the extremely low values of Re, Os, and Ir, in CMS 04071 metal. It is coincidental that the sulfide phase in CMS 04071 exhibits Re above the detection limit, while Re is below detection limit in the metal-sulfide mix, and near detection limit in the metal. Differences between the CMS pallasite, IAB irons, and experimental studies may also be due to different cooling rates, metal composition and thermal histories. In particular, the effect of minor elements such as

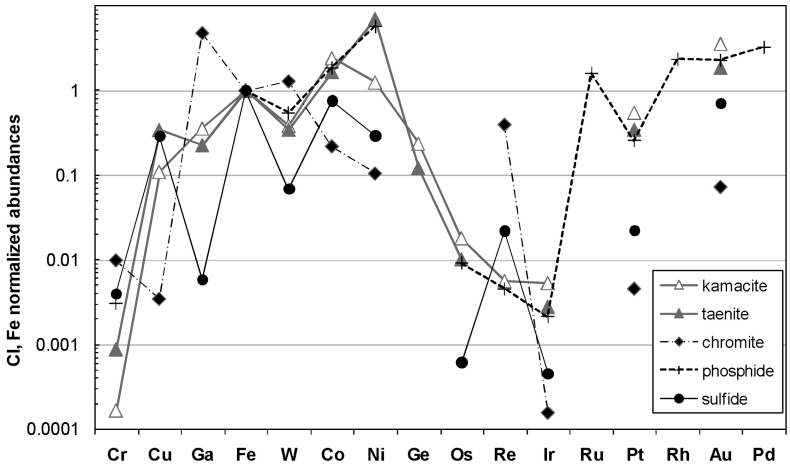

Fig. 7. Trace element abundances for CMS 04071 taenite, kamacite, sulfide, phosphide, and chromite normalized to CI chondrites and Fe (CI chondrite data from tabulation of McDonough and Sun 1995).

Table 4. Trace element analyses for phosphides, in ppm. Italicized values are detection limits reported in place of element concentration.

	Ph 14	Ph 15	T 17	T 17
Cr	*1.9*	*3.4*	19	0.6
Fe	473000	746000	356000	310000
Co	1300	3650	1680	1390
Ni	310000	250000	112000	69000
Cu	*0.2*	*0.3*	88	110
Ga	*0.01*	*0.02*	7.43	8.70
Ge	*0.1*	*0.1*	11.4	12.0
Mo	1	35.3	9.20	2.91
W	0.125	0.199	0.062	0.065
Re	0.0011	0.0007	0.0011	0.0015
Os	*0.008*	0.0172	0.0170	0.0168
Ir	*0.0008*	0.0040	0.0043	0.0043
Pt	0.002	0.99	0.93	1.07
Au	*0.0003*	1.27	1.18	1.77

C, O, and P, on partitioning of the HSE's can be large (Chabot et al. 2003, 2006; Righter 2005). As a result, D values calculated from natural samples should be considered only a rough guide to partitioning behavior in metal/sulfide systems.

Distribution Between Metal and Olivine

$D(HSE)_{metal/olivine}$ measured here are comparable to values reported by Hillebrand et al. (2004) based on analysis of the Milton and Eagle Station pallasites (except for Re which is ~10; Fig. 9b), and to values measured experimentally for siderophile elements (Capobianco and Watson 1982; Schmitt et al. 1989). In addition, we report D(Pt) and D(Au) values that are greater than 10,000, in agreement with experimental studies showing the incompatibility of Pt and Au in olivine (Righter et al. 2004; Jones et al. 2007). In olivines, high HSE abundances measured in other studies may be a product of metal inclusions, though if this is the case, it is unknown whether these inclusions represent a reaction product of the olivines, a trapped phase from the olivine cumulate magma, or a contaminant from the pallasite metal (as in *Santa Rosalia*, Buseck 1977).

Chromite and Phosphide

Chromite contains the highest concentration of Ga and Re of all the phases, consistent with previous studies. Ga is known to be hosted by the spinel structure in general (e.g., Malvin and Drake 1987). Re-rich spinel-structured oxides have been found naturally (Righter et al. 1998; Chesley and Ruiz 1998) and experimentally (Righter and Downs 2001), thus high Re contents in the pallasite chromite are not unexpected, even though Re is in greater concentration in other phases such as metal, sulfide, and olivine. Our measured values of Co (60, 155 ppm) are much higher than those measured in the Brenham pallasite (13 ppm; Davis 1975). No zoning was detected in the chromites, as is apparent with major elements such as Al, Cr, and Ti (J. Boesenberg, personal communication), but the scale of analysis in this

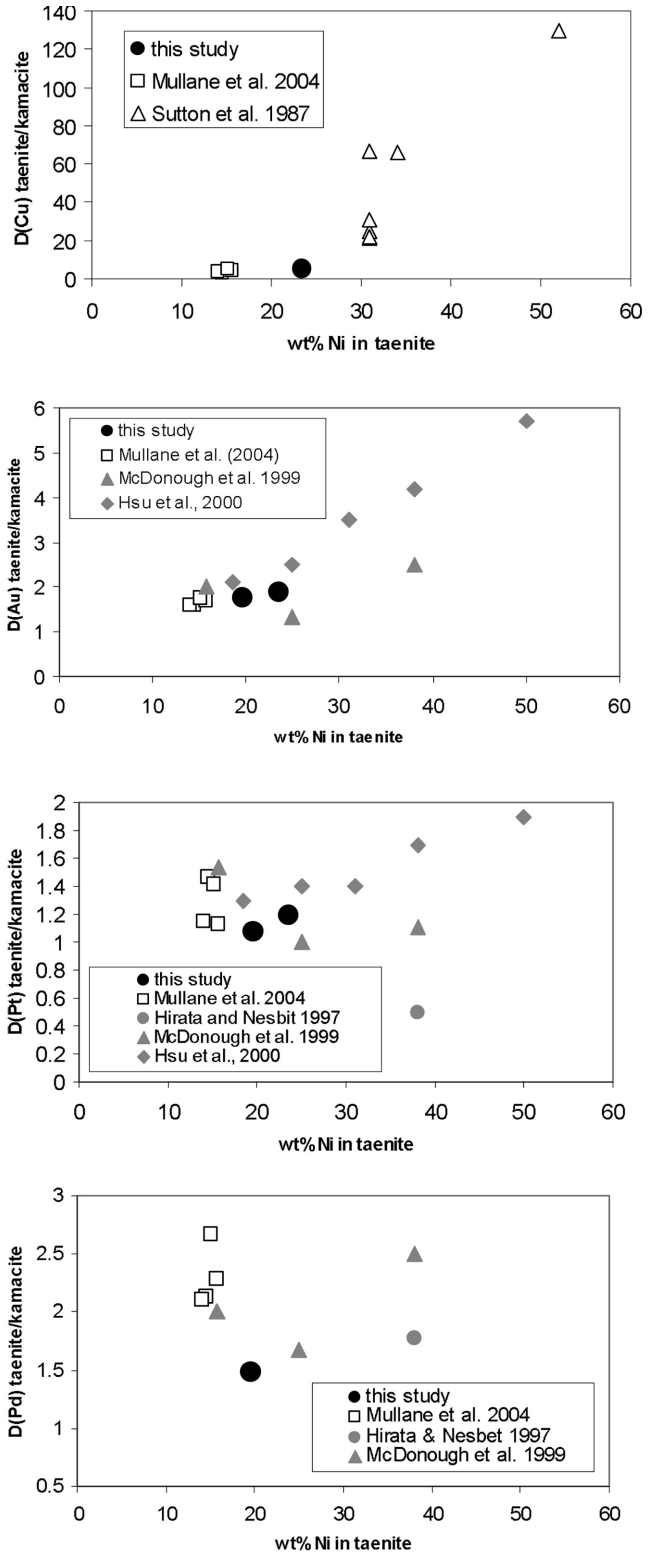

Fig. 8. Comparison of taenite/kamacite distribution coefficients from this study to those measured in previous studies. The variation in D with Ni content of taenite is observed for Cu and Au, but not clear for Pt. For Pd, Ru, Rh, Ir, and Os, the variation is relatively small and our results are consistent with previous studies.

study is larger than the microprobe, thus precluding easy detection of zoning.

Several phosphide grains were analyzed as part of this study. They show a general enrichment in Co and Ga, similar Cr, but lower Cu than those measured in the Brenham pallasite schreibersite (Davis 1975). Gallium contents of the schreibersite are higher than all phases except kamacite, as also measured by Cavell et al. (2004) in Canyon Diablo IAB iron meteorite. In addition, Au is ~4× higher in phosphide than in chromite, and Os has the highest concentration of the HSE (17 ppb) in schreibersite, similar to that found by Shen and Wasserburg (1996) for mineral separates from pallasites (5 to 70 ppb). Mo contents of the phosphide are also high; we could not find any previous measurements of Mo in phosphides from iron meteorites for comparison, so this may be a new finding. An interesting comparison is provided by HSE partitioning between phosphide and metal fremdlinge from Allende CV3 (Campbell et al. 2003) that also show high Mo, but extremely low levels of most other HSE relative to metal. These are general observations that are apparent despite the variability of absolute concentrations; these initial results for a few elements (Ga, Mo, Os, and Au) may justify a more systematic study of phosphides in metal-rich systems to better understand their role in fractionating these elements.

Relation to Other Pallasites

The metal trace element composition and olivine and chromite compositions indicate that the CMS pallasites are part of the Main Group pallasites (Figs. 5 and 6). This group has a distinct metal composition from that of the IIIAB irons (Wasson and Choi 2003). All trace elements suggest that CMS is a Main Group pallasite. Nickel, Co, Ga, Ge show weak compatibility during magmatic evolution, Au shows incompatibility, and Ir and Pt show strong compatibility, and the trends with increasing abundances of Ni are consistent with CMS being part of a fractional crystallization trend. Although a few "anomalous metal" pallasites have similar trace element compositions, Ir, Pt, and Co are lower and Au is higher than those samples (Wasson and Choi 2003).

Olivine Ni and Co contents for Main Group pallasites form part of a wide trend from 10 to ~80 ppm Ni. Although this is a large range of Ni concentrations, the CMS pallasite overlaps with the low end defined by a subset of Main Group pallasites. Looking at Cr contents of olivine leads to a similar conclusion, except that the Cr contents extend to very high values of up to 550 ppm Cr. This may suggest that previous INAA measurements on bulk samples (Davis 1977) were affected by small inclusions of chromite that would increase the Cr contents of the olivine, but not the Co contents. It should also be noted that many measurable trace elements for olivines (Sc, Ga, Cr) are not reported or analyzed in all studies, but would be of great value in evaluating affinities between different groups (Fig. 10).

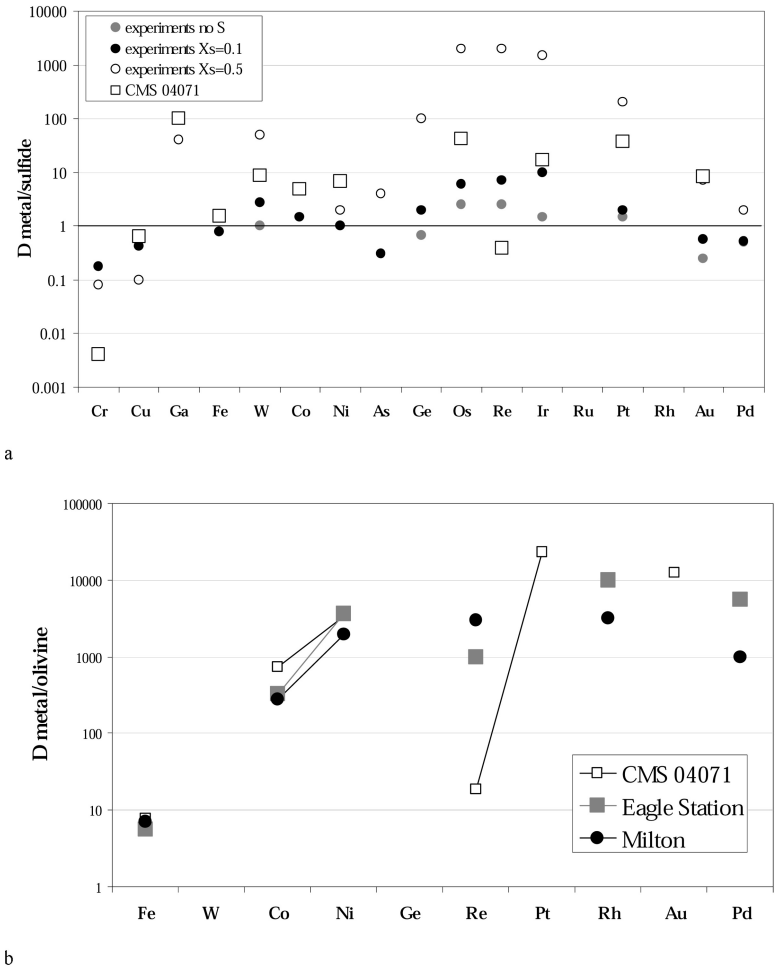

Fig. 9. a) Comparison of CMS 04071 metal and sulfide measurements to partition coefficients from liquid metal-solid metal experiments compiled and reported by Chabot et al. (2003, 2006) and Chabot (2004). Experimental values are shown for systems containing no S, Xs = 0.1 and Xs = 0.5 to illustrate the effect of variable S content on the partition coefficients. In many cases, the values measured for metal/sulfide in CMS 04071 are similar to those values for experimental liquids with Xs = 0.5. b) Partition coefficients of metal/olivine for this study and two other pallasites (Hillebrand et al. 2004).

Even though most trace elements in CMS are consistent with a magmatic fractionation origin for the pallasite metal compositions, there are a few exceptions. The Ge and Ga concentrations in CMS are generally ~10 ppm lower than that measured by Wasson and Choi (2003) for Main Group pallasites. This is inconsistent with their hypothesis that these elements became enriched in the metal via trapped gas pockets from mantle collapse. The lower concentrations would be more consistent with the escape of volatiles from an impact. The recent hypothesis of Asphaug et al. (2006), that a diversity of meteorite types may result from the survival of small objects and chains of objects after hit and run style collisions between planet and embryo-sized objects, may be a more tenable idea for pallasite formation. A variety of physical states of post-impact materials (deformation, spin, volatile-bearing or loss, size, thermal) could be an explanation for the range of pallasite textures (rounded, angular, mixed olivines) and bulk compositions (Main Group, anomalous silicates, anomalous metal and Eagle Station subgroup) of key volatile trace elements such as Ge.

Relation to Other Olivine-Bearing Ultramafic Achondrites

The extensive overlap in olivine trace element composition and oxygen isotopic composition (Goodrich and Righter 2000) between pallasites and the metal- and olivine-rich QUE 93148 ungrouped achondrite suggests that they may be petrogenetically linked. Even though the CMS pallasite olivine Ni and Co concentrations do not overlap with olivine from the QUE 93148 achondrite, they form part of a coherent trend formed by CMS 04071, Main Group pallasites, and QUE 93148. This trend becomes more distinct when olivine Ni and Co contents of olivine-bearing diogenites are considered. These diogenites form a trend that does not overlap the pallasite-QUE trend at all, suggesting a separate and distinct petrogenetic history and evolution for these two bodies (Fig. 10). On the other hand, the different trends could

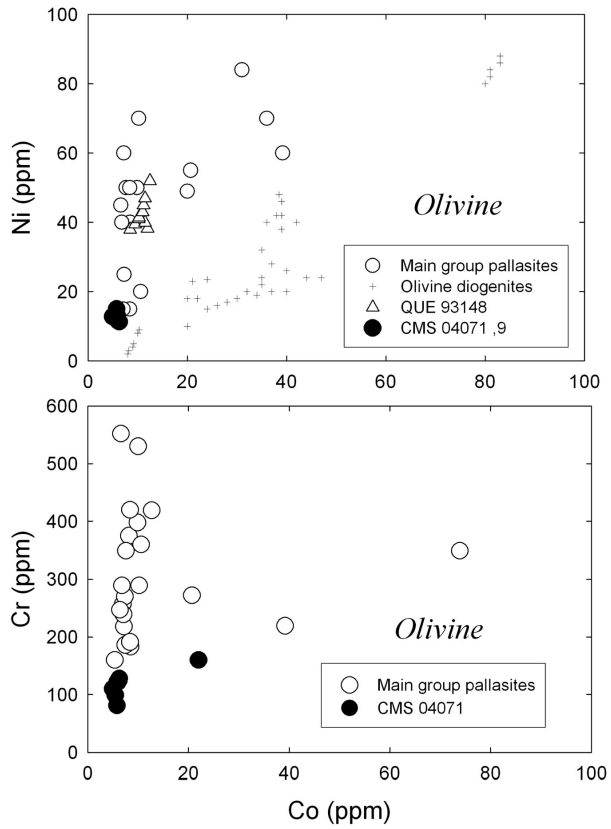

Fig. 10. Olivine Ni (ppm) versus Co (ppm) and Cr (ppm) versus Co (ppm) for many pallasites, olivine-bearing diogenites, and the anomalous ultramafic achondrite QUE 93148 compared with the CMS pallasite. The CMS pallasite have Ni and Co concentrations that overlap those of the low end defined by previous work on pallasites, but do not overlap those of QUE 93148 olivine. Data are from Davis (1977), Shearer et al. (2001, 2007), Hillebrand et al. (2004), and this study.

be formed by different roles for minerals that fractionate Ni and Co, such as olivine, orthopyroxene and spinel (chromite). Future efforts should concentrate on distinguishing the role of these three minerals in the detailed evolution and distribution of these elements as well as any others that can be discriminators such as Sc, Ga, and Cr.

Volatile Element Depletion of Pallasite, HED, and Brachinite Parent Bodies

Differentiated bodies in the inner solar system are distinguished by variable degrees of volatile element depletions, such as K, Na, Rb, Cs, and Ga. Making comparisons between some of these bodies can be difficult due to the very low concentrations of the lithophile volatile elements, for example Na, K, and Rb in phases such as olivine and chromite (in pallasites and brachinites). However, Ga has higher concentrations in chromite and olivine, having an affinity for the spinel structure, and can be used to make a comparison between various basaltic samples and meteorite samples of bodies that contain only olivine or chromite. Partition coefficients for Ga between olivine and chromite and silicate melt are well known from previous studies: D(Ga) chromite/melt = 60 (Righter et al. 2008b) and D(Ga) olivine/melt = 0.3 (Malvin and Drake 1987).

Chromites from the CMS pallasite contain 57 ppm Ga (Table 3), and when coupled with a D(Ga) chromite/melt = 60, yields a Ga content of the melt of ~1 ppm. Similarly, olivines contain 0.07 to 0.09 ppm Ga in olivine, which when coupled with D(Ga) olivine/melt = 0.3, yields a melt Ga content of ~0.3 ppm. These low Ga melt contents, from 0.3 to 1 ppm, are similar to, but slightly lower than the Ga contents of the basaltic eucrites (Warren et al. 1996; Righter and Drake 2000). Correlations between Ga and Ti define depletions of Ga with respect to chondritic values, and when this element pair is considered for the CMS pallasite, the Ga depletion is indeed similar to that defined by eucrites and the HED parent body, and not as high as the values defined by angrites (Kurat et al. 2004).

Brachinites, on the other hand, appear to be slightly less volatile element depleted. Chromites from the brachinites contain 281–357 ppm Ga (Righter et al. 2008), and when coupled with a D(Ga) chromite/melt = 60, yields a Ga content of the melt of ~5 ppm. Similarly, olivines contain up to 0.6 ppm Ga in olivine, which when coupled with D(Ga) olivine/melt = 0.3, yields a melt Ga content of ~2 ppm. These higher Ga melt contents, from 2 to 5 ppm, are intermediate between the Ga contents of the basaltic eucrites and those of Mars and Earth (Righter and Drake 2000).

There is similarity between the CMS pallasite and HED parent body Ga depletions, a feature not shared by the angrites, brachinites, and martian and terrestrial samples. These characteristic Ga depletions indicate that the CMS pallasite and HED parent bodies are associated with a region of the inner solar system whose materials experienced a similar volatile element depletion event that encompassed different parent bodies.

SUMMARY

Closure temperature, texture, and metal-chromite-olivine composition, all indicate that CMS 04071 is a Main Group pallasite. The differences in pallasite and IIIAB iron cooling rates derived from metal and olivine compositions suggests that pallasites formed either on a separate parent body from IIIAB irons, or underwent a significantly different cooling history early in their genesis. The low Ga and Ge concentrations support the hypothesis that CMS 04071 was derived from a parent body formed by planetary embryo impact. In fact, the pallasites may have as many as ten different parent bodies without any strong links to other meteorite groups. Nonetheless, they share a similar volatile element depletion to HEDs that is distinct from other bodies such as Earth, Mars, the Angrite Parent Body (APB), and the Brachinite Parent Body.

Acknowledgments—We wish to thank Georg Ann Robinson for producing the BSE map of CMS 04071,9. Loan Le provided assistance on the electron microprobe. The MWG and Smithsonian Institution allocated the sample. This research was supported by a NASA postdoctoral Fellowship to LRD, a NASA RTOP to K. Righter, and NASA grant NNG06GF50G to M. Humayun. The manuscript benefitted from reviews by Henning Haack, Joe Boesenberg, and Alex Ruzicka. We also thank Alex Ruzicka for editorial handling of this manuscript.

Editorial Handling—Dr. Alex Ruzicka

REFERENCES

Satterwhite C. and Righter K. 2005. *Antarctic Meteorite Newsletter* 28(2).

Ash R. D., Luong M.V., Walker R. J., McDonough W. F., and McCoy T. J. 2007. Trace element fractionation in kamacite and taenite in IVA irons. 38th Lunar and Planetary Science Conference. Abstract #2383.

Asphaug E., Agnor C. B., and Williams Q. 2006. Hit and run planetary collisions. *Nature* 439:155–158.

Boesenberg J. S., Davis A. M., Prinz M., Weisberg M. K., Clayton R. N., and Mayeda T. K. 2000. The pyroxene pallasites, Vermillion and Yamato 8451: Not quite a couple. *Meteoritics & Planetary Science* 35:757–769.

Bunch T. E. and Keil K. 1971. Chromite and ilmenite in non-chondritic meteorites. *American Mineralogist* 56:146–157.

Buseck P. R. 1977. Pallasite meteorites—Mineralogy, petrology, and geochemistry. *Geochimica et Cosmochimica Acta* 41:711–740.

Campbell A. J. and Humayun M. 1999. Trace element microanalysis in iron meteorites by laser ablation ICPMS. *Analytical Chemistry* 71:939–946.

Campbell A. J. and Humayun M. 2005. Compositions of Group IVB iron meteorites and their parent melt. *Geochimica et Cosmochimica Acta* 69:4733–4744.

Campbell A. J., Humayun M., and Weisberg M. K. 2002. Siderophile element constraints on the formation of metal in the metal-rich chondrites Bencubbin, Weatherford, and Gujba. *Geochimica et Cosmochimica Acta* 66:647–660.

Campbell A. J., Simon S. B., Humayun M., and Grossman L. 2003. Chemical evolution of metal in refractory inclusions in CV3 chondrites. *Geochimica et Cosmochimica Acta* 67:3119–3134.

Capobianco C. J. and Watson E. B. 1982. Olivine/silicate melt partitioning of germanium: An example of a nearly constant partition coefficient. *Geochimica et Cosmochimica Acta* 46:235–240.

Cavell R. G., Barnes E. M., Arboleda P. H., Cavell P. A., Feng R., Gordon R. A., and Webb M. A. 2004. An X-ray and electron microprobe study of the Fe, Ni, Ga, and Ge distribution and local structure in a section of the Canyon Diablo iron meteorite. *American Mineralogist* 89:519–526.

Chabot N. L. 2004. Sulfur contents of the parental metallic cores of magmatic iron meteorites. *Geochimica et Cosmochimica Acta* 68:3607–3618.

Chabot N. L., Campbell A. J., Jones J. H., Humayun M., and Agee C. B. 2003. An experimental test of Henry's Law in solid metal-liquid systems with implication for iron meteorites. *Meteoritics & Planetary Science* 38:181–196.

Chabot N. L., Campbell A. J., Jones J. H., Humayun M., and Lauer H. V. Jr. 2006. The influence of carbon on trace element partitioning behavior. *Geochimica et Cosmochimica Acta* 70:1322–1335.

Chesley J. T. and Ruiz J. 1998. Crust-mantle interaction in large igneous provinces: Implications from the Re-Os isotope systematics of the Columbia River flood basalts. *Earth and Planetary Science Letters* 154:1–11.

Davis A. M. 1977. The cosmochemical history of the pallasites. Ph.D. dissertation, Yale University, USA, 355 p.

Goodrich C. A. and Righter K. 2000. Petrology of unique achondrite Queen Alexandra Range 93148: A piece of the pallasite (howardite-eucrite-diogenite?) parent body? *Meteoritics & Planetary Science* 35:521–536.

Greenwood R. C., Franchi I. A., Jambon A., Barrat J. A., Burbine T. H. 2006. Oxygen isotope variation in stony-iron meteorites. *Science* 313:1763–1765.

Hillebrand J. T., McDonough W. F., Walker R. J., and Piccoli P. N. M. 2004. Characterization of the distribution of siderophile and highly siderophile elements in the Milton and Eagle Station pallasites. 35th Lunar and Planetary Science Conference. Abstract #1278.

Hirata T. and Nesbitt R. W. 1997. Distribution of platinum group elements and rhenium between metallic phases of iron meteorites. *Earth and Planetary Science Letters* 147:11–24.

Horn I., Foley S. F., Jackson S. E., and Jenner G. A. 1994. Experimentally determined partitioning of high field strength- and selected transition elements between spinel and basaltic melt. *Chemical Geology* 117:193–218.

Hsu W., Huss G. R., and Wasserburg G. J. 2000. Ion probe measurements of Os, Ir, Pt, and Au in individual phases of iron meteorites. *Geochimica et Cosmochimica Acta* 654:1133–1147.

Humayun M., Simon S. B., and Grossman L. 2007. Tungsten and hafnium distribution in calcium-aluminum inclusions (CAIs) from Allende and Efremovka. *Geochimica et Cosmochimica Acta* 71:4609–4627.

Jones R. H., Wasson J. T., Larsen T., and Sharp Z. D. 2003. Milton: A new unique pallasite. 34th Lunar and Planetary Science Conference. Abstract #1683.

Kurat G., Varela M. E., Brandstätter F., Weckwerth G., Clayton R. N., Weber H. W., Schultz L., Waesch E., and Nazarov M. A. 2004. D'Orbigny: A non-igneous angritic achondrite? *Geochimica et Cosmochimica Acta* 68:1901–1921.

Lauretta D. S., Hill D. H., Della-Giustina D. N., and Killgore M. 2006. The Fukang pallasite: Evidence for non-equilibrium shock processing. 37th Lunar and Planetary Science Conference. Abstract #2250.

Jones J. H., Malavergne V., and Neil C. R. 2007. Crystal field effects and siderophile element partitioning: Implications for Mars HSE geochemistry. Lunar and Planetary Science Conference. Abstract #1170.

Malvin D. J., Wang D., and Wasson J. T. 1984. Chemical classification of iron meteorites. X - Multielement studies of 43 irons, resolution of group IIIE from IIIAB, and evaluation of CU as a taxonomic parameter. *Geochimica et Cosmochimica Acta* 48:785–804.

Malvin D. J. and Drake M. J. 1987. Experimental determination of crystal/melt partitioning of Ga and Ge in the system forsterite-anorthite-diopside. *Geochimica et Cosmochimica Acta* 51: 2117–2128.

Mason B. 1963. The pallasites. *American Museum Novitates* 2163:1–19.

Massalski T. B. and Park F. R. 1964. A study of four pallasites using metallographic, microhardness, and microprobe techniques. *Geochimica et Cosmochimica Acta* 28:1165–1175.

McDonough W. F. and Sun S. S. 1995. The composition of the Earth. *Chemical Geology* 120:223–53.

McDonough W. F., Horn I., Lange D., and Rudnick R. L. 1999.

Distribution of platinum group elements between phases in iron meteorites. 30th Lunar and Planetary Science Conference. Abstract #2062.

Mittlefehldt D. W., McCoy T. J., Goodrich C. A., and Kracher A. 1998. Non-chondritic meteorites from asteroidal bodies. *Planetary materials*, edited by Papike J. J. Reviews in Mineralogy, vol. 36. pp. 4-1–4-195.

Mullane E., Alard O., Gounelle M., and Russell S. S. 2003. LA-ICP-MS study of IIIAB irons and pallasites: HSE behavior during magmatic fractionation. *Meteoritics & Planetary Science* 38: 5119.

Pernicka E. and Wasson J. T. 1987. Ru, Re, Os, Pt, and Au in iron meteorites. *Geochimica et Cosmochimica Acta* 51:1717–1726.

Pouchou J.-L. and Pichoir F. 1991. Quantitative analysis of homogeneous or stratified microvolumes applying the model "PAP". *Electron microprobe quantitation*, edited by Heinrich K. F. J. and Newbury D. E. New York: Plenum Press. pp. 31–75.

Righter K. 2005. Highly siderophile elements: Constraints on Earth accretion and early differentiation. *Earth's deep mantle: Structure, composition and evolution*, edited by J. Bass, R. van der Hilst, Matas J., and Trampert J. AGU Geophysics Monogram Series 160. pp. 201–218.

Righter K., Campbell A. J., Humayun M., and Hervig R. L. 2004. Partitioning of Ru, Rh, Pd, Re, Ir and Au between Cr-bearing spinel, olivine, pyroxene, and silicate melts. *Geochimica et Cosmochimica Acta* 68:867–880.

Righter K., Chesley J. T., Geist D., and Ruiz J. 1998. Behavior of Re during magma fractionation: An example from Volcan Alcedo, Galapagos Archipelago. *Journal of Petrology* 39:785–795.

Righter K. and Downs R. T. 2001. Crystal structures of Re- and PGE-bearing magnesioferrite spinels: Implications for accretion, impacts and the deep mantle. *Geophysical Research Letters* 28: 619–622.

Righter K. and Drake M. J. 2000. Metal/silicate equilibrium in the early Earth—New constraints from the volatile moderately siderophile elements Ga, Cu, P and Sn. *Geochimica et Cosmochimica Acta* 64:3581–3597.

Righter M., Lapen T., and Righter K. 2008. Relationship between HEDs, mesosiderites, and ungrouped achondrites: Trace element analyses of mesosiderite RKPA 79015 and ungrouped achondrite QUE 93148. 39th Lunar and Planetary Science Conference. Abstract #2468.

Righter M., Lapen T., Righter K., and Brandon A. 2008. Partitioning of Hf between chromite and silicate melts: implications for Lu-Hf isotopic systematics of Martian meteorite ALH 84001. *Meteoritics & Planetary Science* 43:5328.

Schmitt W., Palme H., and Wänke H. 1989. Experimental determination of metal/silicate partition coefficients for P, Co, Ni, Cu, Ga, Ge, Mo, W and some implications for the early evolution of the Earth. *Geochimica et Cosmochimica Acta* 53: 173–86

Scott E. R. D. 1977a. Pallasites-metal composition, classification, and relationships with iron meteorites. *Geochimica et Cosmochimica Acta* 41:349–360.

Scott E. R. D. 1977b. Formation of olivine-metal textures in pallasite meteorites. *Geochimica et Cosmochimica Acta* 41:693–710.

Scott E. R. D. 2007. Impact origins for pallasites. 38th Lunar and Planetary Science Conference. Abstract #2284.

Seifert S., O'Neill H. St. C., and Brey G. 1988. The partitioning of Fe, Ni, Co between olivine, metal, and basaltic liquid. *Geochimica et Cosmochimica Acta* 52:603–616.

Shearer C. K., Papike J. J., and Karner J. M. 2001. Chemistry of Olivine from Planetary Materials. Mn/Fe and trace element systematics in an unusual achondrite QUE 93148. 32nd Lunar and Planetary Science Conference. Abstract #1634.

Shearer C. K., Burger P. V., and Papike J. J. 2007. Petrogenetic relationships between diogenites and olivine diogenites: Implications for magmatism on the HED parent body. 38th Lunar and Planetary Science Conference. Abstract #1141.

Shen J. J., Papanastassiou D. A., and Wasserburg G. J. 1996. Precise Re-Os determinations and systematics of iron meteorites. *Geochimica et Cosmochimica Acta* 60:2887–2900.

Shen J. J., Papanastassiou D. A., and Wasserburg G. J. 2002. Re-Os and Pd-Ag systematics in Group IIIAB irons and in pallasites. *Geochimica et Cosmochimica Acta* 66:3793–3810.

Sutton S. R., Delaney J. S., Smith J. V., and Prinz M. 1987. Copper and nickel partitioning in iron meteorites. *Geochimica et Cosmochimica Acta* 51:2653–2662.

Tomiyama T. and Huss G. R. 2006. Minor and trace element zoning in pallasite olivine: Modeling pallasite thermal history. 37th Lunar and Planetary Science Conference. Abstract #2132.

Tomiyama T., Huss G. R., Nagashima K., and Krot A. N. 2007. Ion microprobe analysis of ^{53}Mn-^{53}Cr systematics in pallasite olivines. 38th Lunar and Planetary Science Conference. Abstract #2007.

Ulff-Møller Choi B.-G., Rubin A., Tran J., and Wasson J. T. 1998. Paucity of sulfide in a large slab of Esquel: New perspectives on pallasite formation. *Meteoritics & Planetary Science* 33:221–227.

Warren P. H., Kallemeyn G. W., Arai T., and Kaneda K. 1996. Compositional-petrologic investigation of eucrites and the QUE 94201 shergottite (abstract). 21st Symposium on Antarctic Meteorites. pp. 195–197.

Wasson J. T., Ouyang X., Wang J., and Jerde E. A. 1989. Chemical classification of iron meteorites: XI. Multi-element studies of 38 new irons and the high abundance of ungrouped irons from Antarctica. *Geochimica et Cosmochimica Acta* 53:735–744.

Wasson J. T., Choi B. G., Jerde E. A., Ulff-Møller F. 1998. Chemical Classification of iron meteorites: XII. New members of the magmatic groups. *Geochimica et Cosmochimica Acta* 62:715–724.

Wasson J. T., Lange D. E., Francsi C. A., and Ulff-Møller F. 1999. Massive chromite in the Brenham pallasite and the fractionation of Cr during the crystallization of asteroidal cores. *Geochimica et Cosmochimica Acta* 63:1219–1232.

Wasson J. T. and Choi B.-G. 2003. Main-group pallasites: Chemical composition, relationship to IIAB irons and origin. *Geochimica et Cosmochimica Acta* 67:3079–3096.

Wasson J. T., 1999. Trapped melt in IIIAB irons; solid/liquid elemental partitioning during the fractionation of the IIIAB magma. *Geochimica et Cosmochimica Acta* 63:2875–2889.

Watson H. C., Watson E. B., McDonough W. F., and Ash R. D. 2005. Siderophile element profile measurements in iron meteorites using laser ablation ICP-MS. 36th Lunar and Planetary Science Conference. Abstract #2141.

Watson H. C., Watson E. B., McDonough W. F., and Ash R. D. 2008. Low temperature siderophile element partition coefficients in iron meteorites. 39th Lunar and Planetary Science Conference. Abstract #2374.

Yanai K. and Kojima H. 1995. Yamato 8451: A newly identified pyroxene-bearing pallasite. *Proceedings of the NIPR Symposium on Antarctic Meteorites* 8:1–10.

Yang J. and Goldstein J. I. 2006. Metallographic cooling rates of the IIIAB iron meteorites. *Geochimica et Cosmochimica Acta* 70: 3197–3215.

Yang J., Goldstein J. I., and Scott E. R. D. 2008. Thermal history and origin of the main group pallasites. 39th Lunar and Planetary Science Conference. Abstract #1938.

Ziegler K. and Young E. D. 2007. Pallasite, mesosiderite, and HED Δ^{17}O signatures: The details. 38th Lunar and Planetary Science Conference. Abstract #2021.

APPENDIX

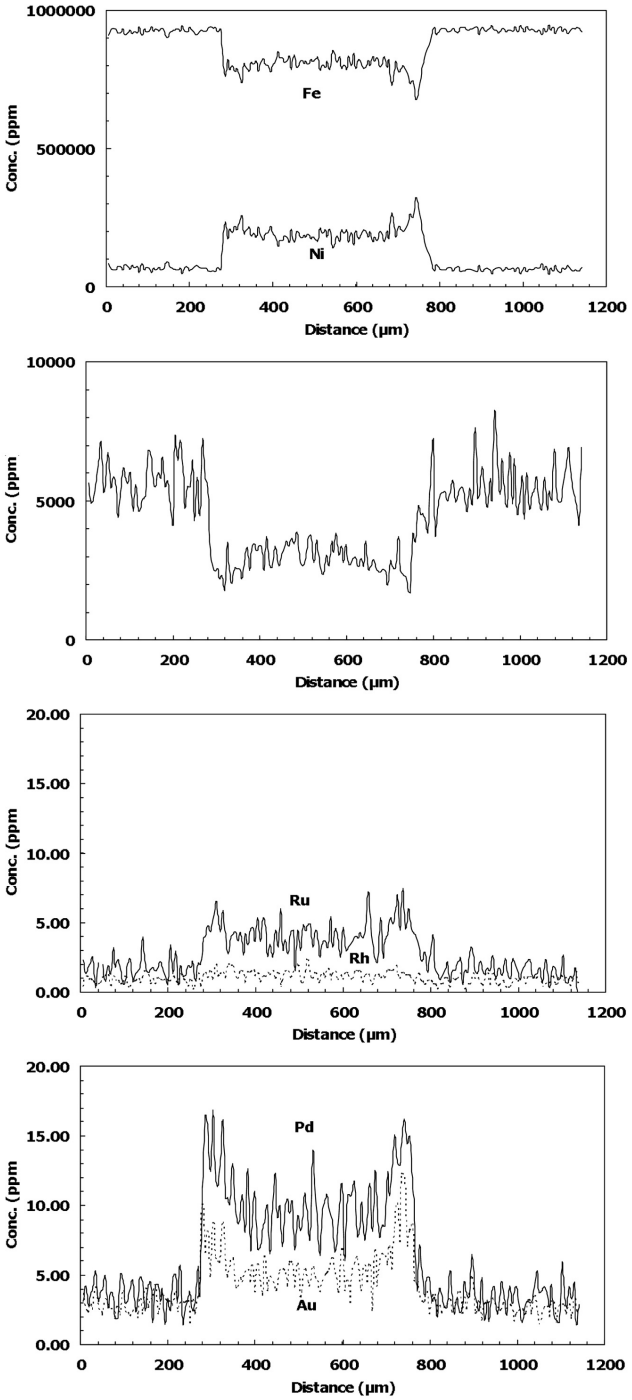

Fig. A1. Trace element analytical track across kamacite and taenite metallic phases (in track # T20), illustrating classic M-shaped patterns for Ni, and corresponding patterns for Co, Ru, Rh, Pd, and Au. Taenite/kamacite partition coefficients for these elements are based on this traverse carried out in high resolution mode; a subset of other elements was measured in lower resolution mode. Both are presented in Table 1.

Table A1. Cumulus Ridge (CMS) pallasite pairing group.

Sample	Mass (kg)
CMS 04 061	8.465
CMS 04 062	15.315
CMS 04 063	6.1883
CMS 04 064	19.195
CMS 04 065	5.738
CMS 04 066	5.877
CMS 04 067	7.5619
CMS 04 068	20.425
CMS 04 069	44.700
CMS 04 070	3.5158
*CMS 04 071	2.1101
CMS 04 072	2.3129
CMS 04 073	0.9282
CMS 04 074	0.3257
CMS 04 075	0.009592
CMS 04 076	0.008252
CMS 04 077	9.625
CMS 04 078	5.6952
CMS 04 079	12.550
Total mass (kg)	170.545944

Table A2. Electron microprobe analyses of minerals in CMS 04071.

	Olivine	Chromite	Sulfide	Phosphide	Kamacite	Taenite
SiO_2	40.65	n.d.				
$Ti(TiO_2)$	n.d.	0.04	0.02			
Al_2O_3	0.00	1.73				
$Cr(Cr_2O_3)$	0.02	67.02	0.09			
Fe(FeO)	11.50	22.62	61.01	47.42	92.8	76.1
Mn(MnO)	0.27	–	0.025			
MgO	47.58	5.40				
CaO	n.d.	–				
$P(P_2O_5)$	n.d.	–		15.17		
S	n.d.	–	36.39			
Ni(NiO)	0.02	–	0.06	34.75	6.8	23.6
Co	n.a.	–				
Total	100.06	97.21	97.53	97.37	99.6	99.7

Ti, Cr, Fe, Mn, P, and Ni values are reported as elemental for sulfide, phosphide, and metal, and as oxide for olivine and chromite.

Table A3. Trace element concentrations for metals in ppm. Italicized values are detection limits reported in place of element concentration. Labels correspond to locations shown in Fig. 5.

	M46 Kamacite	M 47 Kamacite	M 48 Kamacite	M 49 Kamacite	T 20 Kamacite	M 52 Taenite	M 16 Plessite	T 20 Plessite	M 50 metal Sulfide mix	Sul 57 Sulfide
Cr	7.6	*3.5*	*3.2*	*2.5*	*1.4*	92	*25*	*27*	*5.9*	602
Fe	928000	928000	930000	915000	929000	761000	884000	801000	654000	596000
Co	6030	5700	5570	6080	5560	3230	5670	2880	2710	1190
Ni	65500	66600	65000	78600	65600	236000	110000	197000	343000	10000
Cu	73	71	61	87	*0.1*	140	*2*	*2*	190	110
Ga	18.6	18.4	16.3	19.2	*0.008*	9.2	*0.16*	*0.18*	7.2	0.18
Ge	38.1	38.2	37.2	37.1	*0.05*	16.7	*0.94*	1.03	11.6	*0.25*
Mo	5.00	4.86	4.98	7.22	4.16	28.5	11.3	5.52	42.1	*4*
W	0.177	0.177	0.171	0.177	0.141	0.124	0.167	0.138	0.111	0.020
Re	0.0010	0.0005	0.0009	0.0014	0.0651	*0.0013*	*0.004*	0.0570	*0.008*	0.0025
Os	0.0324	0.0351	0.0395	0.0519	0.0572	0.0176	0.0370	0.0521	0.0106	*0.0011*
Ir	0.0101	0.0097	0.0108	0.0150	0.0409	0.0048	0.0101	0.0324	0.0031	0.0007
Pt	2.11	2.39	2.38	3.33	1.62	1.26	2.20	1.92	0.82	0.07
Au	2.59	2.62	2.34	2.71	2.77	1.09	2.78	5.48	0.83	0.31